When Size Matters: Active Area Dependence of PEFC Cold Start Capability

Author(s):
Biesdorf, Johannes; Stahl, Peter; Siegwart, Muriel; Schmidt, Thomas; Boillat, Pierre

Publication date:
2015-01

Permanent link:
https://doi.org/10.3929/ethz-b-000105023

Originally published in:
Journal of the Electrochemical Society 162(10), https://doi.org/10.1149/2.0871510jes

When Size Matters: Active Area Dependence of PEFC Cold Start Capability

J. Biesdorf,[a,z] P. Stahl,[b] M. Siegwart,[a] T. J. Schmidt,[a,c,*] and Pierre Boillat[a,d]

[a]*Electrochemistry Laboratory (LEC), Paul Scherrer Institut (PSI), 5232 Villigen PSI, Switzerland*
[b]*Elring Klinger AG, 72581 Dettingen/Erms, Germany*
[c]*Laboratory of Physical Chemistry, ETH Zürich, 8093 Zürich, Switzerland*
[d]*Neutron Imaging and Activation Group (NIAG), Paul Scherrer Institut (PSI), 5232 Villigen PSI, Switzerland*

Understanding the freezing mechanism of liquid water within polymer electrolyte fuel cells (PEFC) is crucial for its commercialization for mass market. Although various publications investigated the cold start capability of PEFCs, contradictory behaviors during cold starts at freezing temperatures have been published in literature. Interestingly, differences can be mainly identified between large and small size fuel cells: the latter have a significantly higher cold start capability than large size fuel cells. In order to understand the influence of different active areas, we present measurements of cold starts performed with cells sizes of 1 and 50 cm^2 using the same materials, including a large count of experiments (>200) on the 1 cm^2 cells to perform statistical analysis. The cold start capability is strongly reduced with an increasing size of the active area, and the operating times changes from stochastic values for small cells to reproducible values for large cells. Both effects can be explained by the higher probability of the aggregate state transition from super-cooled water to ice in large cells. Consequently this paper highlights the implications of downscaling PEFCs to draw conclusions for technical relevant cold-starts.
 [DOI: 10.1149/2.0871510jes] All rights reserved.

Manuscript submitted April 14, 2015; revised manuscript received July 28, 2015. Published August 10, 2015.

Within the last decade, polymer electrolyte fuel cells (PEFCs) have proven their potential to replace fossil fuel based power generators for stationary as well as mobile applications. However, operation under ambient environment[1,2] requires various enhancements regarding degradation, efficiency as well as cold start capability at subfreezing temperatures, where product water risks to freeze. Subzero cold start investigations have been widely reported.[3–8] Mainly two experimental protocols are used: *Free-heating* and *isothermal start-up*. *Free-heating start-ups* investigate the capability of start-up of a fuel cell, by heating up the cell with the waste heat of the electrochemical reaction.[9] This technique is technically relevant for commercial applications and has been mostly studied on technical fuel cells or fuel cell stacks.[5,9–14] Such measurements usually aim to validate if the full subzero start-up strategy is valid, i.e. if the stack reaches temperatures above zero degrees before failure occurs due to the blocking of the cell by frozen water. However, they give little information about the actual failure mechanisms. Therefore, isothermal start-ups in moderate sub-freezing temperatures are often reported,[3,4,6,8,15–20] where the PEFC is maintained at a constant subfreezing temperature during its operation and a better scientific understanding of the freezing mechanism is obtained.

In literature, strongly differing explanations can be found concerning the ongoing processes during a cold start. Agreement can be found on the fact, that at the beginning of a cold start, the membrane takes up a certain amount of water, which can be identified by a dropping ohmic resistance. After a certain time, the membrane resistance stabilizes, which can be explained by a saturation of water content inside the membrane. However, a strong disagreement exists on the aggregate states of water inside the membrane. Some studies based on differential scanning calorimetry (DSC)[21–23] conclude that part of the water in the membrane is freezable, while other studies using X-ray scattering contradict these findings.[24,25]

Besides product water which is diffusing back into the membrane, water is present in the electrode. Concerning the aggregate state of water inside the electrode, contradictory findings have been published. Some studies[16,20,26–28] claim that all product water produced during the start-up freezes inside the catalyst layer of the cathode. After filling a certain amount of the pore space with ice, the reactant gases are blocked, leading to a breakdown of the electrochemical reaction. Such claims were contradicted by visualization experiments,[3,6] which identified liquid water inside the GDL and flow channels. Furthermore, if all the product water would be systematically frozen, a reproducible operation time proportional to the quantity of water needed to block the electrode would be expected. However, within previous measurements of our group,[3] strong variations of the operation times have been identified. This variation can be explained by the production of super-cooled water[6] which is in good agreement to studies performed with imaging[3,6,8,29] where super-cooled water has been undoubtedly identified inside the GDL and flow fields. Besides the proof by imaging, Oberholzer et al.[3] have shown that the phase transition was triggered by a mechanical shock onto the PEFC.

Super-cooled water remains liquid below the thermodynamic melting point.[30–33] This aggregate state was identified as a metastable state of water and remains only with a certain probability in its liquid state.[34] The phase transition is triggered by agitation, mechanical shock or friction,[35] or by the contact with a seed such as a small ice nuclei. The ability of super-cooling water was identified as being a function of several parameters: the cluster/droplet volume and the temperature of subcooling. The cluster volume is of high importance, as reported in a recently published theoretical analysis of Ishikawa et al.[36] They have shown that super-cooled water is thermodynamically stable until it reaches a critical droplet size which is in the order of 10 nm at −10°C and 3 nm at −30°C. Below this critical droplet diameter, super-cooled water remains in a meta-stable state. Consequently, as state of the art catalyst have pores in the order of magnitude of 30 nm, frozen water may exist inside the catalyst layer.[37,38]

The influence of the operating temperature on the capability for cold starts has been studied. Tabe et al.[15] have performed isothermal start-ups at two different cell temperatures (−20°C, −10°C) with a fuel cell of 25 cm^2. They obtained reduced operation times with decreased temperatures. This is in good agreement with Refs. 3 and 8 where also reduced operational times have been identified with lower cell temperatures. These findings are also consistent with the existence of super-cooled water, as the phase transition between super-cooled and ice is more probable at lower temperatures.[39]

In literature, subfreezing startup studies are reported with various sizes of active areas ranging from 0.16 cm^2,[8] 0.5 cm^2,[3,29] 2.5 cm^2,[28] 5 cm^2,[17] 13 cm^2,[6] 25 cm^2,[7,9,15,26] 33 cm^2,[40] 40 cm^2,[5] 46 cm^2[41,42] to 220 cm^2.[18] Interestingly, the studies identifying liquid water inside the GDL and flow field, concern exclusively experiments with relatively small fuel cells (active areas below 15 cm^2), whereas high reproducibility and frozen electrodes have been found inside larger size fuel cells. This indicates that the freezing process might be related to the size of the active area. Here, we present the experimental results of

*Electrochemical Society Active Member.
[z]E-mail: johannes.biesdorf@psi.ch

subzero isothermal start-up experiments with two different cell sizes of 1 and 50 cm^2. Using the statistical distribution of operating time for small cells (1 cm^2) we calculate the operating time as a function of the cell area, closing an important understanding gap between the stochastic operating time of small cells and the deterministic operating times of larger cells.

Experimental and Modelling

Cell designs.— The experiments were performed on two different cells designs. Cell type 1 is a differential fuel cell with an active area of 1 cm^2 operating at high stoichiometries[43,44] to ensure a homogenous distribution of temperature, humidification and gas composition along the channels. The cell has 5 parallel flow channels (1 cm long, 1 mm wide and 0.55 mm deep), and is made of gold coated aluminum. A more detailed description can be found in Ref. 45. In order to study cell-to-cell variations, 5 identical cells were studied. The distribution of operation times was found to have no correlation with the number of freezing cycles previously performed, indicating that there was no degradation effect affecting the operation time.

Cell type 2 is a 50 cm^2 fuel cell operated with technical stoichiometries. The bipolar plates are made of graphite with a single serpentine flow field. The bipolar plates are compressed between aluminum endplates with integrated cooling channels and additional electrical heaters for a fine control of the temperature. Further details can be found in Ref. 46.

In order to enable comparable conditions, identical catalyst coated membranes (CCM) (Primea 5710, Gore Ltd., USA) were used with Pt-loadings of 0.1 mgPt cm^{-2} on the anode and 0.4 mgPt cm^{-2} on the cathode side. Commercial GDLs were used from the SGL Carbon Group Series 24BC[47] with a hydrophobic coating of 5 wt% PTFE inside the GDL and 23 wt% PTFE inside the microporous layer (MPL).[48] In both experiments, the sub-freezing temperature was controlled via a thermal bath, operated with a mixture of 50% Ethylene-Glycol and water. A precise temperature control was achieved with several local heaters on both PEFCs.

Experimental protocol.— All tests were performed with a slightly enhanced gas pressures. The differential cell was studied at 1.1bar_{abs} on both sides, whereas the 50 cm^2 cell was operated at 1.15bar_{abs} at the anode and 1.25bar_{abs} on the cathode side, respectively. The cell flows were set to 0.1 Nl/min on the anode and cathode side for both cell designs which translates into stoichiometries of 140/60 for the 1 cm^2 and 2.8/1.2 for the 50 cm^2. The following start-up protocol was used which is similar as for the experiments previously published in Ref. 3:

1. *Drying*: The cells were dried with nitrogen on both sides, until the high frequency resistance (measured at 5 kHz) reached 0.5 Ohm cm^2.
2. *Preconditioning*: The membrane was preconditioned under nitrogen humidified with 50% RH on both sides for 20 minutes.
3. *Cool down*: The cells were cooled down, to the desired temperature, while the gas flows were stopped in order to prevent drying out of the membrane.
4. *Feed gas*: After stabilizing the temperature, unhumidified reactant gases (hydrogen and air) were fed until the cell voltage reached a voltage above 0.9 V during 5s.
5. *Apply current*: The current was linearly increased over 60s to reach 0.1 A cm^{-2} (see Figure 1). Afterwards, the cells were operated in galvanostatic mode until the cell voltage dropped below 0.2 V where the current was stopped. In case the cells were not frozen, the step was interrupted after 2 hour.
6. *Heat up*: In the final step, the cells were heated up to 25°C.

This protocol was performed at various temperatures with the two different cell sizes. As identified during the experiments, the differential cell shows highly scattered operation times, whereas the lab-scale PEFC gives more reproducible results. Consequently, a certain number of repetitions have been performed on the small scale PEFC in order to get statistical information. The exact number of cold starts performed at each temperature is listed in Table I.

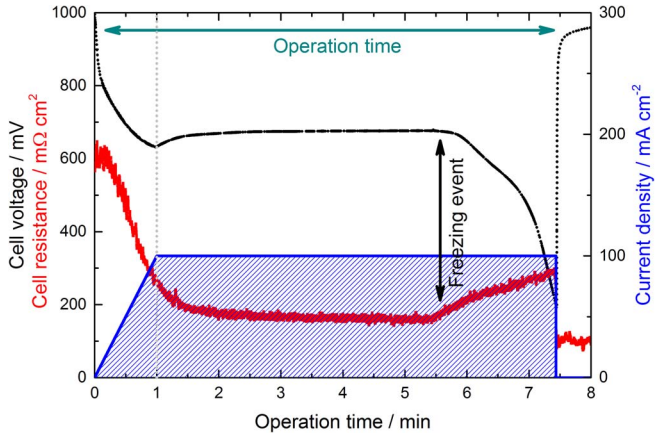

Figure 1. Experimental data of a typical cold start performed at −7.5°C with a 1 cm^2 fuel cell.

Data processing.— In literature, different methodologies are used to characterize the cold start ability of the fuel cell. The freezing capability can be characterized with the operational time,[3] which is the time from start of current production until the cell voltage drops below 0.2 V (see Figure 1). Other similar definitions such as the specific accumulated charge[40–42] or the specific amount of water produced[7,26] during the cold start are also used. Within this paper the cold start ability is analyzed based on the specific charge produced until the cell potential drops below 0.2 V (see freezing event in Figure 1) as well as on the operation time. The specific accumulated charge q_c is calculated on the basis of the current density i during the operation time t (blue shaded area in Figure 1):

$$q_c(T) = \int_0^t i\, dt \qquad [1]$$

In order to get a characteristic indicator for each temperature, a median value is calculated, which will be called *accumulated charge* henceforth. The lower and upper quartiles (interval between 0.25 and 0.75 of all measurements values) represent the error bars shown hereafter (see Figure 2).

Simulation.— In order to get a better understanding of the influence of the active area on the operation time, a Monte Carlo simulation was performed. The simulation parameters were fitted to the experimental data obtained with the differential fuel cells at −7.5°C (see orange curve in Figure 2), as the highest numbers of repetitions were performed with this configuration (see Table I). As five different cells with identical materials were tested, the simulation accounts for local

Table I. Number of cold starts performed at the individual temperatures.

Temperature°C	Cell type 1: 1 cm^2	Cell type 2: 50 cm^2
−15	9	
−10	33	
−7.5	284	
−7		1
−6		1
−5	72	1
−4		1
−3		1
−2		1

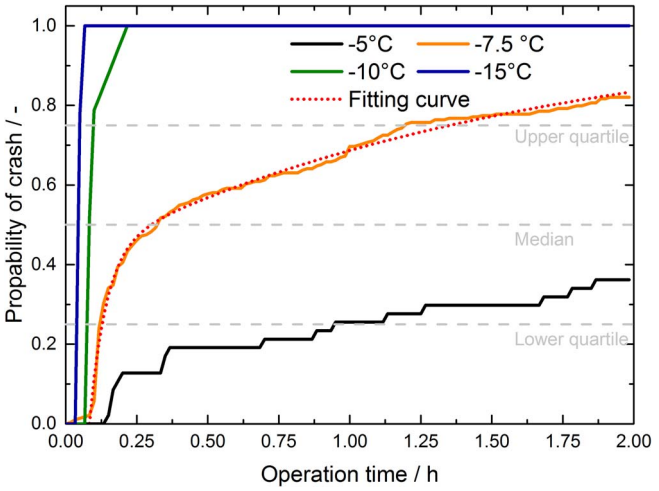

Figure 2. Measured probability distributions of a cell failure with a cell of 1 cm^2 at various subfreezing temperatures.

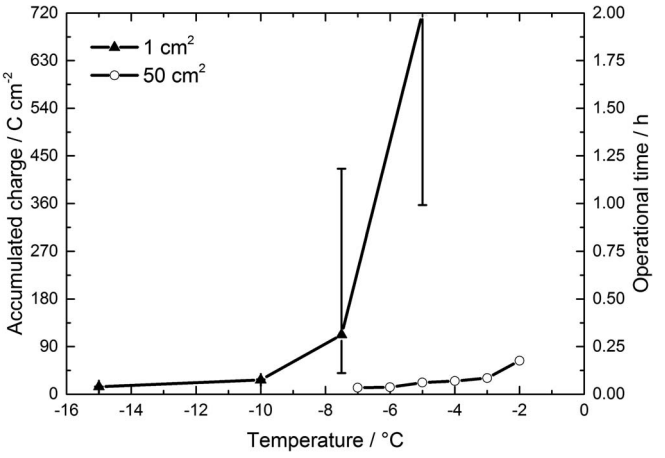

Figure 3. Experimental results of the cold start capability of two different cell sizes at various subfreezing temperatures. The points show median values, error bars indicate the upper and lower quartiles.

variations of the material composition (e.g. specific points in the carbon fibers which can act as a "seed" for the freezing) which influences the cold start capability.

This distribution can be used for calculations of increased cell sizes under two assumptions: every 1 cm^2 portion of the larger cells has the same probability distribution to freeze as a 1 cm^2 fuel cell; the water is considered to form a continuous network, thus the freezing in any of the portions of the cell will propagate to the entire cell.[49,50] This assumption is based on theoretical percolation studies[51] which describe the capillary water transport within the GDL as being independent on the direction, resulting in highly interconnected water cluster within the GDL. These theoretical studies are in good agreement with high resolution X-Ray Tomography data of operating fuel cells.[52]

Under these circumstances, it is reasonable to assume that each small section of the cell is independent from the other in terms of freezing probability, and the operating time of a cell with an area of n cm^2 is calculated as the minimum value of n independent variables following the probability distribution of freezing in the 1 cm^2 cell. If the event of freezing is considered to have a constant probability for a given time interval, the corresponding probability distribution on the operating times should be an exponential. However, within fuel cells the probability of failure cannot be assumed to be constant and two types of failures have to be distinguished. The first type of cell failure occurs within the first 10 minutes with a high probability, as the amount of water inside the GDL and CCM increases. The second type occurs after 10 minutes of operation occurs with a much lower probability, after the water distribution has stabilized.[3] This probability distribution can be best modelled as a sum of two exponentials:

$$p = a \cdot \left(1 - e^{-\frac{t-t_0}{t_1}}\right) + (1-a) \cdot \left(1 - e^{-\frac{t-t_0}{t_2}}\right), \qquad [2]$$

with a, t_0, t_1, t_2 being fitting constants. In order to get sufficient statistics, 100,000 cold starts were simulated for each of the six cell sizes (1, 2, 5, 10, 25, 50 cm^2) chosen for the simulation. The fitting parameters can be found in Table II.

Table II. Fitting parameters used for the Monte Carlo simulation.

	a	t0	t1	t2
Overall	0.479	300	348.743	7687.044
Cell 03	0.872	300	180.564	3075.107
Cell 05	0.072	300	1	6416.205

Results

Experimental results.— Figure 3 depicts the experimental results obtained with the two different cell setups as a function of its isothermal start-up temperature. The calculated points inside the graphic represent the median values over all cold starts performed for a certain cell size and temperature. It can be seen that the median value of the charge produced during the cold start decreases with decreasing temperatures. The differential cell shows at all temperatures the highest operational times and charge produced, whereas the cell with 50 cm^2 shows a significantly lower cold start capability. In Figure 2 it can be seen for the small scale PEFC, that more than 25% of the cells at −7.5°C and more than 75% of the cells at −5°C did not fail within 1 h. In contrast, the PEFC of 50 cm^2 failed within less than 15 min of operation for all temperatures – even with temperatures as high as −2°C. These results highlight that the size of the active area has a significant influence on the cold start capability.

Furthermore it is worth noticing, that the differences between the two cell configurations are amplified with increasing temperatures, whereas the cells converge to a lower limit of the accumulated charge with decreasing temperature. Interestingly, this limit is already reached at around −6°C at a cell size of 50 cm^2, whereas the small scale cell reaches this lower limit not before −10°C. From Figure 2, it can be seen that the minimum operation time of the 1 cm^2 cell decreases with decreasing temperatures.

The trends observed also agree with literature.[3,5,15] Oberholzer et al.[3] performed measurements with a 0.5 cm^2 differential PEFC with similar operational times compared to the 1 cm^2 in Figures 2 and 3. Tabe et al.[15] obtained operational times of around 3 minutes at −10°C with a 25 cm^2 PEFC; Jiao et al.[5] operated a cell of 40 cm^2 for less than 3 minutes at −10°C, which perfectly fit into the data of Figure 3. The cell of 0.16 cm^2 of Mayrhuber et al.[8] could have been operated for longer operational times compared to the experimental data of the 1 cm^2.

The cell of 50 cm^2 shows a smooth temperature dependency of the accumulated charge without any significant outliers (see Figure 3). Although only one experiment at each temperature has been performed with this cell size (see Table I), the continuous trend indicates a more repeatable start-up behavior. In contrast, the small scale cell shows a high variability especially at higher subfreezing temperatures (see Figure 2), whereas more reproducible data is obtained at lower temperatures.

In order to understand the influence of cell-to-cell variations on the overall probability distribution, the individual distributions of the five 1 cm^2 fuel cells are shown in Figure 4. It can be seen, that significant differences are obtained between the cells with median values ranging from less than 15 minutes to more than 1 h. However, all cells except

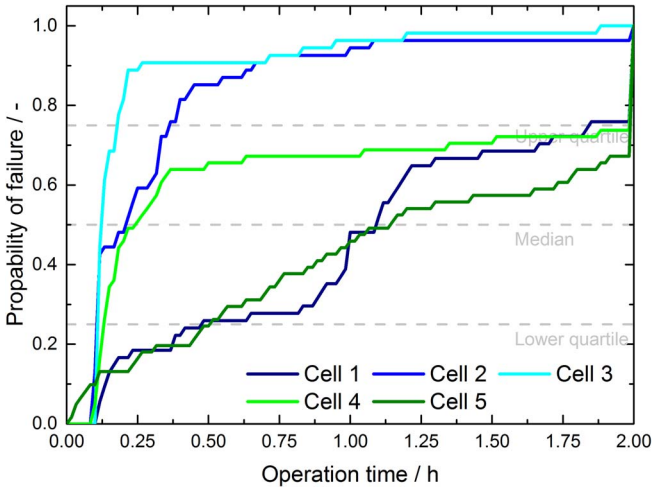

Figure 4. Probability distributions of a cell failure of the five identical 1 cm^2 PEFC at −7.5°C.

cell 5 show a minimal operation time of 5 minutes, which corresponds to 27 Ccm^{-2}. Consequently, the cell-to-cell variations have a strong influence on the freezing behavior of cell with an active area of 1 cm^2.

Modelling results.— In order to understand the impact of cell size on subzero start-up capability, a Monte Carlo simulation was performed based on the experimental data obtained with the five identical 1 cm^2 cells at −7.5°C. Figure 5 shows the results of the simulation based on the statistics obtained with all five cells, and compares the results to the same simulation based on the statistics obtained with the cells having the best (cell 5) and worst (cell 3) start up capabilities. As the model assumes that the probability curve of 1 cm^2 holds for every cm^2 inside a fuel cell of increased cell size, the probability of failure increases with increasing size of the active area. At cell sizes above 10 cm^2, the operation times converge toward a lower limit of 5 minutes, which corresponds to the parameter t_0 of the fitting curve of the experimental data (see Eq. 2). In order to account for the influence of material variations of the 1 cm^2 portions in large size fuel cells, the simulation based on all five cells represents the most realistic case for larger fuel cells. However, the curve of cell 5 represents the distribution with the highest start-up capability found within our experiments. It can be seen that the start-up capability is increased within cell sizes below 10 cm^2, whereas no improvement can be obtained at bigger cell sizes. Nevertheless, all these simulations are in good agreement with

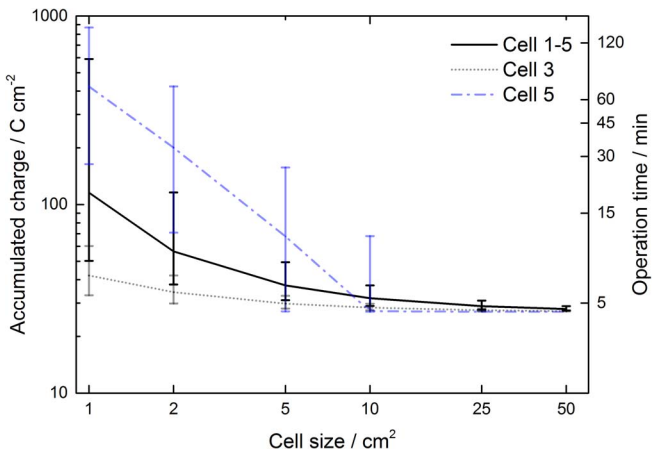

Figure 5. Accumulated charge and operation time as depicted from Monte-Carlo simulation based on the experimental statistical data shown in Figure 4 for different cell sizes at −7.5°C and 0.1 Acm^{-2}.

the experimental results obtained with the 50 cm^2 in Figure 3, where operation times around 3 minutes were obtained.

Furthermore, Figure 5 clearly shows that the variability of the cold starts decreases with increasing cell size. At a size of 1 cm^2 a confidence interval of 540 Ccm^{-2} is obtained, whereas 0.6 Ccm^{-2} is obtained at 50 cm^2. This correlates with our experimental data obtained in Figure 3, where more repeatable isothermal start-ups have been measured with the lab-size fuel cell, whereas highly scattered operational times were obtained with the differential cell above −10°C.

Discussion

Operation time.— As has been shown in Figures 2 and 3, cells with reduced dimensions can be operated for a longer time at subfreezing conditions. This trend is in good agreement with the numerical results obtained in Figure 3. The explanation of this effect is given by the phase transition of super-cooled water into ice. As has already been shown in literature on small scale fuel cells,[3,29] water is condensing in its super-cooled aggregate state under subfreezing conditions. This aggregate state is metastable[30,34] and its phase transition can be induced in different ways (e.g. agitation, mechanical shock, friction or melts[35]). One of these transition mechanisms have been shown for fuel cells in Ref. 3 where the freezing of a fuel cell was triggered by inducing a mechanical shock onto an operating fuel cell. The initiated freezing propagates along the water cluster. As a water cluster extends over a large volume inside the cell,[53] the entire cell freezes within a short time. Within our experiments, the cells were not exposed to any kind of mechanical shocks. Consequently, the phase transition occurs randomly and large fuel cells having a larger water volume have a much higher probability of freezing.

The results of our simulation indicates that the stochastic nature of the water-ice transition is not incompatible with the more repeatable operation times observed with larger cells: above a critical size of approximately 10 cm^2, the freezing probability become high enough so that the operation time is given by deterministic factors (accumulation of water in the membrane, filling of the electrode). This is in good agreement with literature where stochastic freezing times are obtained with small scale fuel cells[3,8,54] and deterministic operation times with larger fuel cells.[5,7,9,15,26,40–42]

Figures 2 and 3 show a decreased cold start ability with decreasing subfreezing temperatures. This effect can be explained with the higher probability of an aggregate state transition with decreasing temperature.[30–33] As the probability distribution reaches its maximum already at an early state, the differences between the cell sizes become smaller. In contrast, under relatively small subfreezing temperatures, the differences of the probability distributions become more dominant.

Cell-to-cell variations.— Within our experiments we have identified significant cell-to-cell variations. These variations may results from various sources. One potential explanation would result from inhomogeneities of the coating, which strongly affect the nucleation rate.[36] Another explanation is the presence of "seeding points" like fiber breaks, asperities or micro cracks. These inhomogeneities can act as seeds for crystal growths.[55] Within large size fuel cells, these variations are spread across the active area leading to an increased probability encountering a seed. However, the simulation of larger cells based on the statistical data obtained with the best of our differential cells indicates clearly improved startup capability for sizes up to 10 cm^2. It must be reminded that state-of-the-art materials are not optimized for the stability of super cooled water, and that an optimized material might have far better properties that the best sample measured here. By understanding which feature of the material promotes the freezing and how to avoid such features, there is a huge potential of improvement of the cold-start capability – possibly also for larger fuel cells.

Lower limit of charge produced.— Within our experiments (see Figure 3), a minimal operation time was identified for both cell configurations. A possible explanation is the water uptake of the mem-

brane and the ionomer inside the electrode. However, as can be seen in Figure 1, the ohmic resistance stabilizes already after around 1.5 minutes corresponding to a production of 6 Ccm^{-2}. The remaining part can be explained by the fact that a certain time is necessary until the catalyst layer is filled with enough ice to block the access of reactants. This mechanism can be observed in the voltage profile in Figure 1 where a progressive voltage drop can be identified after the freezing event occurs. However, the time until the catalyst layer is filled with ice is dependent on the saturation pressure and the gas flow. As the water uptake of the gas is reduced at lower temperatures, less water/ice can be removed in the gas phase which results in a decreased operation time (see Figure 3). Furthermore, the cell with 50 cm^2 was operated under technical stoichiometries, which results in a reduced water uptake along the channel. This effect can be clearly identified in Figure 3, where water tends to freeze immediately below $-7.5°C$ at a cell size of 1 cm^2 and $-3°C$ at a cell size of 50 cm^2. For technical applications, high stoichiometries may extend the minimal cold start capability to several minutes within technical PEFCs.[56]

Conclusions

For the first time, the influence of the active area on the freezing mechanism was investigated systematically. Two different cell setups having different sizes of the active areas (1, 50 cm^2) were studied experimentally under subfreezing conditions. Furthermore, a Monte-Carlo simulation was performed based on the experimental data obtained for the 1 cm^2 cell, in order to extrapolate the freezing behavior to larger active areas. The following new key findings were obtained within this paper:

- The probability of freezing increases with the cell area, resulting in long and stochastic operation times for small cells and short and reproducible operation times for large cells. Consequently, conclusions from most publications performed on small scale PEFCs cannot be directly extrapolated to automotive cells in the order of several hundreds of cm^2.
- Cell-to-cell variations have a significant influence on the cold start capability of small scale fuel cells. Although the impact of the sample variability is, according to our simulation, limited to cell sizes up to 10 cm^2, optimized materials might further reduce the probability of freezing and improve the cold-start capability of larger cells.
- Despite the large cell-to-cell and experiment-to-experiment variations for small cells, the minimal operation times converge to a value consistent with the operation time of large cells, which can be explained by quantity of water uptake by the membrane and electrode until the latter is blocked.

Acknowledgments

This work was carried out with the support of the European Community. We appreciate the support of the European Research Infrastructure H2FC (funded under the FP7 specific programme Capacities, grant Agreement Number 284522). The Commission for Technology & Innovation and the Swiss Competence Center for Energy Research (SCCER): *Efficiency in Mobility* and the SCCER: *Heat & Electricity Storage* are greatly acknowledged for supporting this work.

References

1. J. Biesdorf, N. Zamel, and T. Kurz, *J Power Sources*, **247**, 339 (2014).
2. K. Sekizawa, N. Kitamura, K. Manabe, Y. Nonobe, M. Kizaki, and K. Kojima, *ECS Transactions*, **33**, 1947 (2010).
3. P. Oberholzer, P. Boillat, R. Siegrist, R. Perego, A. Kästner, E. Lehmann, G. G. Scherer, and A. Wokaun, *Journal of The Electrochemical Society*, **159**, B235 (2011).
4. A. D. Santamaria, J. Bachman, and J. W. Park, *Electrochim Acta*, **107**, 327 (2013).
5. K. Jiao, I. E. Alaefour, G. Karimi, and X. Li, *International Journal of Hydrogen Energy*, **36**, 11832 (2011).
6. Y. Ishikawa, H. Harnada, M. Uehara, and M. Shiozawa, *J Power Sources*, **179**, 547 (2008).
7. K. Tajiri, Y. Tabuchi, and C.-Y. Wang, *Journal of The Electrochemical Society*, **154**, B147 (2007).
8. I. Mayrhuber, F. Marone, M. Stampanoni, T. J. Schmidt, and F. N. Büchi, *ChemElectroChem* (2015).
9. Q. G. Yan, H. Toghiani, Y. W. Lee, K. W. Liang, and H. Causey, *J Power Sources*, **160**, 1242 (2006).
10. M. Sundaresan and R. M. Moore, *J Power Sources*, **145**, 534 (2005).
11. E. Schiesswohl, T. von Unwerth, F. Seyfried, and D. Bruggemann, *J Power Sources*, **193**, 107 (2009).
12. F. Jiang, W. Fang, and C.-Y. Wang, *Electrochim Acta*, **53**, 610 (2007).
13. R. K. Ahluwalia and X. Wang, *J Power Sources*, **162**, 502 (2006).
14. R. Fu, U. Pasaogullari, D. S. Hussey, D. L. Jacobson, and M. Arif, *ECS Transactions*, **11**, 395 (2007).
15. Y. Tabe, M. Saito, K. Fukui, and T. Chikahisa, *J Power Sources*, **208**, 366 (2012).
16. E. L. Thompson, J. Jorne, W. Gu, and H. A. Gasteiger, *Journal of The Electrochemical Society*, **155**, B625 (2008).
17. C. Chacko, R. Ramasamy, S. Kim, M. Khandelwal, and M. Mench, *Journal of The Electrochemical Society*, **155**, B1145 (2008).
18. E. Pinton, Y. Fourneron, S. Rosini, and L. Antoni, *J Power Sources*, **186**, 80 (2009).
19. S. H. Ge and C. Y. Wang, *Electrochim Acta*, **52**, 4825 (2007).
20. S. Ge and C.-Y. Wang, *Electrochemical and Solid-State Letters*, **9**, A499 (2006).
21. A. Siu, J. Schmeisser, and S. Holdcroft, *The journal of physical chemistry. B*, **110**, 6072 (2006).
22. E. L. Thompson, T. W. Capehart, T. J. Fuller, and J. Jorne, *Journal of The Electrochemical Society*, **153**, A2351 (2006).
23. H. Yoshida and Y. Miura, *J Membrane Sci*, **68**, 1 (1992).
24. M. Pineri, G. Gebel, R. J. Davies, and O. Diat, *J Power Sources*, **172**, 587 (2007).
25. H. Mendil-Jakani, R. J. Davies, E. Dubard, A. Guillermo, and G. Gebel, *J Membrane Sci*, **369**, 148 (2011).
26. K. Tajiri, Y. Tabuchi, F. Kagami, S. Takahashi, K. Yoshizawa, and C. Y. Wang, *J Power Sources*, **165**, 279 (2007).
27. Z. M. Wan, H. W. Chang, S. M. Shu, Y. X. Wang, and H. L. Tang, *Energies*, **7**, 3179 (2014).
28. J. Mishler, Y. Wang, P. P. Mukherjee, R. Mukundan, and R. L. Borup, *Electrochim Acta*, **65**, 127 (2012).
29. J. Biesdorf, P. Oberholzer, F. Bernauer, A. Kaestner, P. Vontobel, E. H. Lehmann, T. J. Schmidt, and P. Boillat, *Phys Rev Lett*, **112** (2014).
30. L. Hawkes, *Nature*, **123**, 244 (1929).
31. E. J. Langham and B. J. Mason, *Proceedings of the Royal Society A: Mathematical, Physical and Engineering Sciences*, **247**, 493 (1958).
32. S. C. Mossop, *Proceedings of the Physical Society. Section B*, **68**, 193 (1955).
33. E. K. Bigg, *Proceedings of the Physical Society. Section B*, **66**, 688 (1953).
34. O. Mishima and H. E. Stanley, *Nature*, **396**, 329 (1998).
35. *Crystallization*, J. Mullin, Butterworth-Heinemann (2001).
36. Y. Ishikawa, M. Shiozawa, M. Kondo, and K. Ito, *Int J Heat Mass Tran*, **74**, 215 (2014).
37. T. J. Dursch, G. J. Trigub, R. Lujan, J. F. Liu, R. Mukundan, C. J. Radke, and A. Z. Weber, *Journal of The Electrochemical Society*, **161**, F199 (2014).
38. T. J. Dursch, M. A. Ciontea, C. J. Radke, and A. Z. Weber, *Langmuir : the ACS journal of surfaces and colloids*, **28**, 1222 (2012).
39. P. G. Debenedetti, *Journal of Physics: Condensed Matter*, **15**, R1669 (2003).
40. M. Oszcipok, A. Hakenjos, D. Riemann, and C. Hebling, *Fuel Cells*, **7**, 135 (2007).
41. M. Oszcipok, M. Zedda, D. Riemann, and D. Geckeler, *J Power Sources*, **154**, 404 (2006).
42. M. Oszcipok, D. Riemann, U. Kronenwett, M. Kreideweis, and A. Zedda, *J Power Sources*, **145**, 407 (2005).
43. I. A. Schneider, M. H. Bayer, and S. von Dahlen, *Journal of The Electrochemical Society*, **158**, B343 (2011).
44. P. Boillat, Advanced characterization of polymer electrolyte fuel cells using high resolution neutron imaging in *PHD Thesis, Eidgenössische Technische Hochschule ETH Zürich, Nr. 18397*, *PHD Thesis, Eidgenössische Technische Hochschule ETH Zürich (Nr. 18397)*, Zürich (2009).
45. P. Oberholzer, P. Boillat, R. Siegrist, A. Kastner, E. H. Lehmann, G. G. Scherer, and A. Wokaun, *Electrochem Commun*, **20**, 67 (2012).
46. P. Stahl, J. Biesdorf, P. Boillat, J. Kraft, and K. A. Friedrich, *Journal of the Electrochemical Society*, **162**, F677 (2015).
47. SGL TECHNOLOGIES GmbH, GDL 24 & 25 Series Gas Diffusion Layer, Technical data sheet, in (2014).
48. R. Fluckiger, S. A. Freunberger, D. Kramer, A. Wokaun, G. G. Scherer, and F. N. Buchi, *Electrochim Acta*, **54**, 551 (2008).
49. R. Lin, Y. M. Weng, Y. Li, X. W. Lin, S. C. Xu, and J. X. Ma, *International Journal of Hydrogen Energy*, **39**, 16025 (2014).
50. K. Jiao, I. E. Alaefour, G. Karimi, and X. Li, *Electrochim Acta*, **56**, 2967 (2011).
51. P. K. Sinha and C. Y. Wang, *Electrochim Acta*, **52**, 7936 (2007).
52. J. Eller, J. Roth, R. Gaudenzi, S. Irvine, F. Marone, M. Stampanoni, A. Wokaun, and F. N. Büchi, *ECS Transactions*, **50**, 477 (2013).
53. J. Eller, T. Rosén, F. Marone, M. Stampanoni, A. Wokaun, and F. N. Büchi, *Journal of The Electrochemical Society*, **158**, B963 (2011).
54. J. Biesdorf, P. Oberholzer, F. Bernauer, A. Kaestner, P. Vontobel, E. Lehmann, T. J. Schmidt, and P. Boillat, *ECS Transactions*, **58**, 309 (2013).
55. J. Hallett, *Journal of the Atmospheric Sciences*, **21**, 671 (1964).
56. Q. Yan, H. Toghiani, Y.-W. Lee, K. Liang, and H. Causey, *J Power Sources*, **160**, 1242 (2006).